AAS 20-132

EFFECT OF SPACECRAFT PARAMETERS ON IDENTIFICATION OF DEBRIS STRIKES IN GN&C TELEMETRY

Anne Aryadne Bennett[*†], **and Hanspeter Schaub**[‡]

Debris strikes on operational spacecraft are becoming more common due to increasing numbers of space objects. Sample return missions indicate hundreds of minor strikes, but rigorous analysis is often only performed when a strike causes an anomaly in spacecraft performance. Developing techniques to identify and assess minor strikes that do not immediately cause anomalous behavior can help to validate models for debris populations, perform risk assessments, and aid in attribution of future anomalies. This study uses a spacecraft dynamics simulation to determine the effects of minor debris strikes as observed in attitude control system (ACS) telemetry. A variety of filters are applied to a range of ACS telemetry points to identify subtle strikes in noisy telemetry. A series of trades is conducted to examine the effects of spacecraft parameters on strike detectability and assessment accuracy. Traded parameters include spacecraft size, telemetry rate, and telemetry noise. The results from these trades are presented and the implications for the strike detection and assessment capabilities of spacecraft are discussed.

INTRODUCTION

The population of trackable fragmentation debris has more than doubled in the past 25 years[1]. This is especially concerning because while trackable debris can be avoided by maneuvering satellites, most fragmentation events also release clouds of debris too small to track. The Space Surveillance Network tracks debris down to around 10 cm in LEO and 70 cm in GEO[2], but a $<$1 cm piece of debris can cause catastrophic damage to a spacecraft if it hits a sensitive component[3], as illustrated by Figure 1(a). As of January 2019 there are approximately 34,000 debris objects greater than 10 cm in orbit, but there are approximately 900,000 objects between 1 cm and 10 cm[4]. Therefore, well under 10% of the potentially hazardous debris population is tracked.

The situation is especially dire in GEO where many valuable spacecraft are located. Because GEO is not reached by ground-based radar and there are no sample return missions the small debris environment is largely unknown. NASA's orbital debris model, ORDEM3.0, only models debris down to 10 cm in GEO leaving a significant population of potentially harmful debris that is entirely uncharacterized. Even that 10 cm boundary is an extension from debris measurements; the GEO debris models are based on measurements taken by the MODEST telescope which measured pieces $\sim$30 cm and larger[5]. This might account for the abrupt anomalies that several GEO spacecraft have experienced in recent years. For example, in April 2019 Intelsat-29e experienced an abrupt anomaly resulting in a fuel leak and shed debris, culminating in the total loss of the satellite. The failure review board concluded that the anomaly was caused by either a particle strike or an electrostatic discharge event coupled with an existing harness flaw[6]. In other events, such as the Telkom-1 mishap, ground-based telescopes have recorded satellites spontaneously spewing clouds of debris and contributing to the untrackable debris population.

However, not all debris strikes are fatal. In August of 2016 the Sentinel-1A spacecraft experienced an anomaly consisting of an abrupt attitude perturbation (Fig. 1(b)) coupled with a slight orbit change and

[*]Graduate Research Assistant, Colorado Center for Astrodynamics Research, University of Colorado Boulder, 3775 Discovery Dr, Boulder, CO, 80303.

[†]Mission Systems Engineer, Northrop Grumman Space Systems, 45101 Warp Dr, Dulles, VA, 20166.

[‡]Glenn L. Murphy Chair of Engineering, Professor, Colorado Center for Astrodynamics Research, University of Colorado Boulder, 3775 Discovery Dr, Boulder, CO, 80303.

simultaneous decrease in solar power output. On-board cameras confirmed a debris strike on the solar array. However, the solar array strike was non-catastrophic and operations continued nominally[7]. Similar events have been detected on a NASA spacecraft, where anomalous behaviors have been noticed and attributed to debris strikes; however the effects were recoverable and operations continued nominally[8]. In addition to these large and obvious strikes, small strikes occur on spacecraft without even perturbing operations. Sample return missions such as the Long Duration Exposure Facility and the Hubble solar arrays have cataloged hundreds to thousands of small impact craters after a few years on orbit (Figure 1(c))[9].

(a) Tank rupture[10]

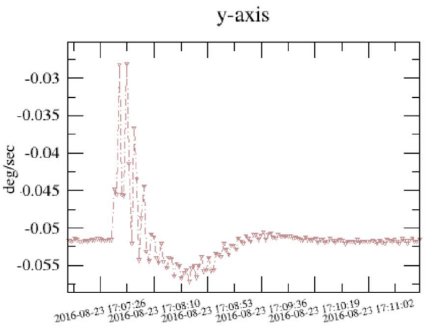

(b) Telemetry from Sentinel-1A strike[7]

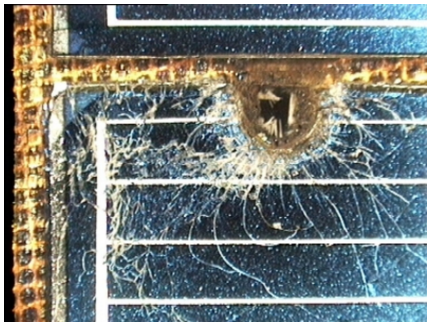

(c) Strike on Hubble solar array *Source: ESA Website*

Figure 1. Examples of small debris impact effects. The tank in a) was impacted by a 2 mm aluminum sphere. The hole in c) is 2.5 mm

Other constellations have experienced events like Sentinel-1A, and a recent report by the NASA Engineering and Safety Center (NESC) incorporated these events into a study comparing observed anomalies to failures predicted using current debris models (ORDEM3.0). The NESC report assessed reported vs. predicted failures for several LEO satellite systems. For one LEO constellation seven events had been observed where satellites experienced sudden unexpected movements thought to be caused by debris. These movements consisted of abrupt changes in satellite mean altitude and/or rotation rates. Comparing these and other events to predicted events, the NESC report found very low correlation between the on-orbit events and the ORDEM3.0 predictions. ORDEM3.0 predicts a substantially higher risk of failures than these LEO systems have experienced[11]. This indicates that current LEO debris models are overly conservative, which is burdensome for ongoing programs as it makes it difficult to show compliance with debris mitigation standards. One of the recommendations of the NESC report is to collect data on satellite orbital perturbations and momentum changes. This paper develops techniques to accomplish this by applying various filters to attitude control system (ACS) telemetry to identify and assess debris strikes.

Some key related work has been done by ExoAnalytic Solutions on detecting 'momentum impulse transfer events' on GEO spacecraft using their global telescope network. They have proven a capability to detect orbit perturbations with in-track velocity changes of 0.2 - 10 mm/s[12]. Some of these are explained with rigorous high-fidelity modeling of solar radiation pressure, but others remain unexplained and could be caused by on-board systems or, potentially, debris impacts. Similarly, ongoing work at the Institute for Defense Analyses is developing methods to calculate the size of untrackable debris impacts based on small changes in satellites' mean altitude[13]. A recent study by ESA conducted at the Ernst-Mach-Institut assesses the momentum transferred during small hypervelocity impacts on spacecraft materials via modeling and test and then develops software to simulate the dynamic response of the a spacecraft to these disturbances. Measurements are planned for an upcoming mission which will derive the momentum transmitted into the spacecraft by microparticle impacts based on these models and analysis[14]. Bennett and Schaub applied some of the techniques used in this paper to telemetry from NASA spacecraft, specifically the Solar Dynamics Observatory (SDO) and the Magnetospheric Multiscale Mission (MMS), and successfully identified instances of unexpected abrupt angular momentum transfer indicative of particle strikes[15].

The goal for this study is to characterize the effect of spacecraft parameters on the accurate identification and assessment of minor debris strikes. A spacecraft dynamics simulation is used to model the effect of debris strikes on ACS telemetry. The numerical simulation models a 3-axis controlled rigid-body spacecraft with four reaction wheels maintaining pointing along a reference trajectory. Debris strikes are applied to the simulation while state noise and measurement noise obfuscate the spacecraft's response to the strikes. The details of this simulation development are discussed in Bennett et. al.[16], while the Analysis Methods section shows the key results to provide context for this study.

Several algorithms are tested to determine their ability to detect and assess small strikes in the simulated noisy telemetry. Algorithms to detect debris strikes are run on three telemetry points: the inertial angular momentum, the attitude error, and the rate error. Two types of algorithms are run on each telemetry point: a simple algorithm that requires minimal *a priori* knowledge of the spacecraft and has a low computational burden, and a refined algorithm that uses knowledge of the spacecraft's characteristics and has more significant computational requirements. These algorithms are discussed in the Analysis Methods section

The performance of these algorithms is characterized via a series of trade studies. First, three design points are developed using three sizes of spacecraft to investigate the effect of spacecraft size on strike detectability. Then a trade is conducted to assess the effects of telemetry rate on each algorithm. Next, the noise in the telemetry is varied to assess the effects of telemetry noise on algorithm performance. First the noise in all telemetry points is scaled together, then the noise in individual points is varied to compare the effects on performance of the various algorithms. Finally some small trades are conducted to characterize the effects of additional parameters: spacecraft inertia, reaction wheel inertia, and initial reaction wheel speed. The results are discussed in the context of lessons learned while applying these techniques to real telemetry[15] to provide an assessment of the potential real-world utility of these techniques.

ANALYSIS METHODS

Simulated Debris Strikes

When a debris strike is applied to the spacecraft dynamics simulation as discussed in Bennett et. al[15], the results are as shown in Figure 2. The spacecraft's rate increases abruptly as the strike imparts an impulsive torque, and the attitude error begins to increase. The spacecraft's attitude control system responds by spinning up the reaction wheels to correct the drift, so the rate and attitude errors return to zero. However, this spin-up results in a step upwards in the spacecraft's inertial angular momentum, which persists. Note the similarities between the Sentinel-1A debris strike telemetry shown in Figure 1(b) and the rate telemetry from the simulation. Figure 2 shows the spacecraft's truth state, with no state or measurement noise added to the simulation. Once noise is added it obfuscates these signals, so algorithms are developed to process the noisy telemetry and identify these features even when the strikes are subtle compared to the noise floor. The spacecraft and noise parameters used in this study are given in the appendix. These represent the default baseline parameters; the trades vary these parameters as specified in each trade.

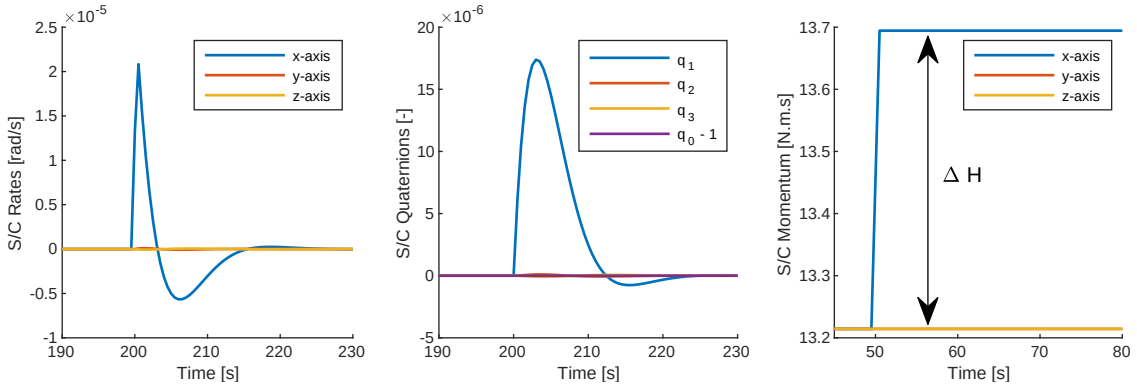

(a) Rate Telemetry (b) Attitude Telemetry (c) Momentum Telemetry

Figure 2. Response of spacecraft to simulated debris strike

Refined Strike Detection Algorithms

Two types of algorithms are used to detect strikes: matched filters and sequential probability ratio tests (SPRTs). The matched filters are a standard digital signal processing technique. They are applied to the rate and attitude telemetry, since those show an expected signal when a debris strike occurs. Matched filters return an increased output when the filter is run on telemetry where the signal is present under the noise. The truth response of the spacecraft is used as the signal to be detected, called a wavelet. This wavelet is cross-correlated with noisy telemetry as shown in Figure 3. Note that the raw telemetry drifts upwards and downwards when the strike is applied, as expected, but the change is insignificant compared to the normal noise in the telemetry. However, when the expected wavelet is used in a matched filter the filter shows a distinct response at the time of the strike.

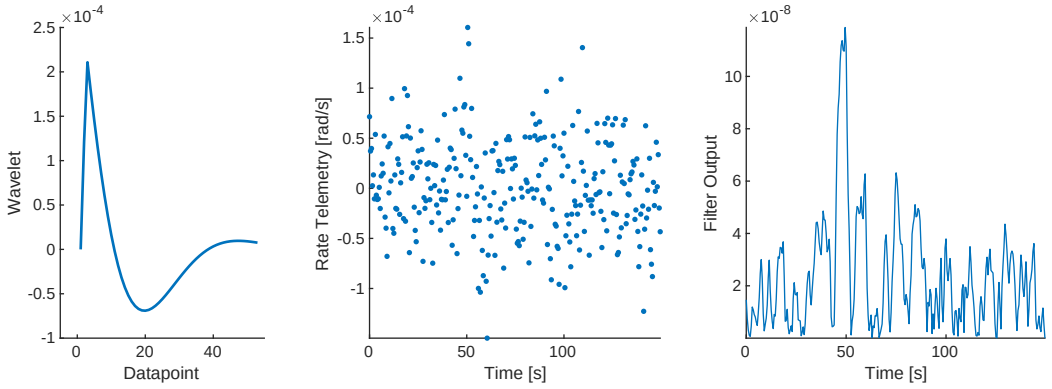

(a) Wavelet (b) Rate Telemetry (c) Filter Output

Figure 3. Matched filter accentuates strike at t=50 s

For the momentum telemetry, an SPRT is used to highlight the step upwards in momentum produced by the strike. The Cumulative Sum SPRT is used, and is implemented as described by Bennett et. al.[16]. The algorithm calculates the likelihood ratio for each datapoint in a sliding window and compares the likelihood under the null hypothesis (no strike) to the likelihood under the alternative hypothesis (strike occurred). As such, there are two tuning parameters: the length of the sliding window and magnitude of strike for the alternative hypothesis, ΔH. Figure 4 shows the algorithm applied to telemetry, where a change in momentum occurred at t=300s but is small compared to the noise in the telemetry. Figure 4(b) shows the underlying probability distribution parameters overlaid on the data. The output of the SPRT in Figure 4(c) shows a distinct spike when the change occurs. Note that since this algorithm computes a probability density function twice for each datapoint in each window it is by far the most computationally intensive.

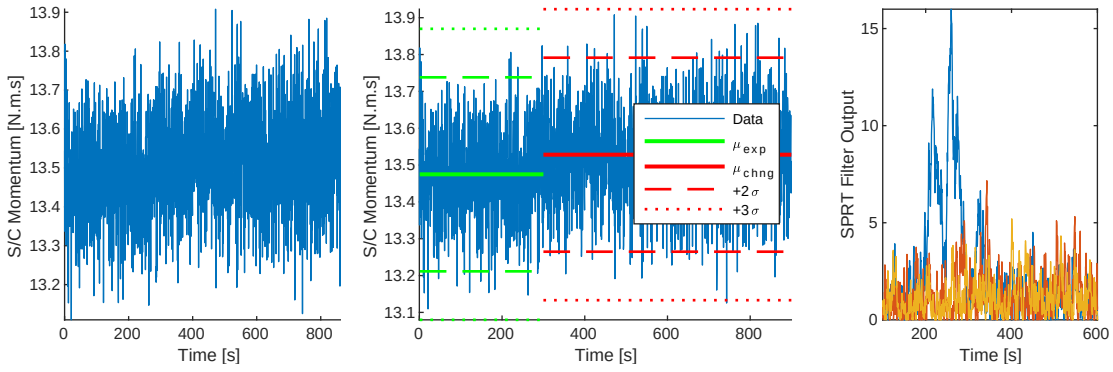

(a) Raw Telemetry (b) With Distribution (c) Filter Output

Figure 4. SPRT accentuates strike at t=300 s

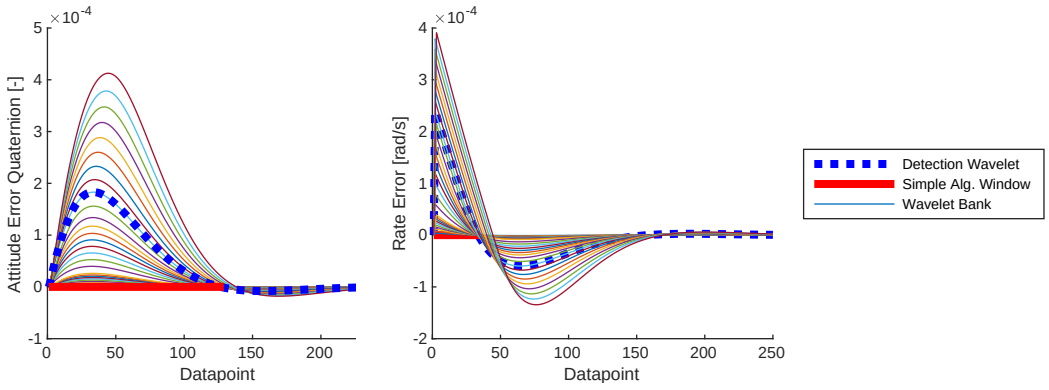

(a) Attitude Wavelets (b) Rate Wavelets

Figure 5. Wavelet banks for strike size estimation, with detection wavelet for matched filter and summation window for simple filters

Simple Strike Detection Algorithms

The refined strike detection algorithms rely on exquisite knowledge of the spacecraft's response characteristics or on computationally intensive algorithms. While a higher telemetry rate improves performance, state of health telemetry is typically downlinked at fairly low rates but processed at much higher rates on board. Therefore, simple algorithms are also investigated which are computationally simple enough to easily run onboard and require minimal tuning. For the attitude and rate telemetry, the simple filter just sums the attitude or rate error over a window corresponding to the duration of the initial peak in the response (Figure 5 - thick solid red line). For the momentum telemetry, the average momentum over 200 datapoints is differenced with the average momentum for the preceding 200 datapoints, so a higher difference in averages indicates that a change has occurred.

Strike Size Estimation Algorithms

Once a strike is detected the next task is to estimate the size of the strike. To estimate the change in angular momentum imparted on a given axis two methods are compared. In the first, a bank of matched filters of varying strike sizes (Figure 5) is compared to the attitude and rate telemetry, and the mean-squared error difference between the telemetry and each wavelet is computed. The minimum mean squared error wavelet is selected as the most likely strike size. This technique is applied to both simple and refined algorithms at the time of peak filter output during a strike. Alternately, the momentum processing algorithms use the difference in average momentum before and after the detected strike to estimate the size. The details of these techniques are discussed by Bennett et. al.[16] To compare these techniques the standard deviation of the error between the estimated strike size and the true strike size is used to express the strike estimation accuracy.

TRADE STUDIES

To characterize the performance of the algorithms under various combinations of parameters a process is developed outputs the ΔH detection threshold and estimation accuracy for a given scenario. First, a simulation is run in which a series of strikes with increasing magnitude is applied to the simulation (Figure 6(a)). The filters are run and each filter's peak output is recorded along with the applied strike size. A positive 2nd-order polynomial is fitted to this data to develop a relationship between the strike size and filter output (Figure 6(b)). Peaks below the noise floor are ignored when fitting. Then a long simulation is run with no strikes. The filters are run on this data producing a population of filter output data when no strikes are present. A Kernel distribution is fitted to this data since standard distributions often fit poorly, especially on the tails. A false alarm rate of one per day is selected as the strike detection threshold - for a given telemetry data rate, a probability of 1/(number of telemetry points in a day) is used as the desired probability of false alarm (P_{fa}). The threshold for strike detection is calculated based on the fitted probability density functions given the desired

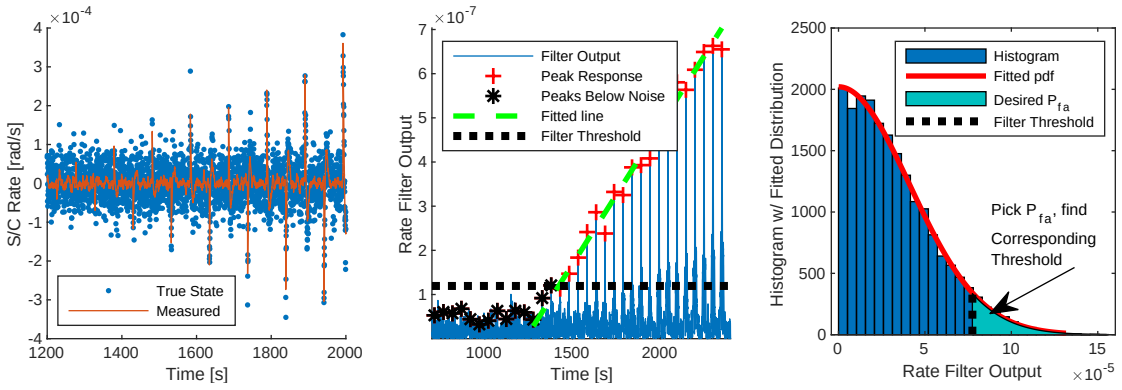

(a) Rate Telemetry w/ Strikes (b) Correlate Filter Output to ΔH (c) Fitting noise distribution

Figure 6. Process for determining ΔH threshold

P_{fa} (Figure 6(c)). This filter output threshold is mapped to a ΔH threshold using the relationship between strike size and filter output. Note that minor changes in the probability density functions or curve fitting can lead to changes in the thresholds, leading to somewhat noisy measurements of the threshold. Therefore, when evaluating the results the major trends are the desired outcome, exact thresholds vary slightly across runs producing some noise in the results. To quantify the estimation accuracy a series of strikes is applied to the simulation that are 1.5x the ΔH threshold, then the estimation accuracy for these strikes is calculated as described in the section on Strike Size Estimation Algorithms.

Note that some parameters are fixed in order to reduce the scope of the problem to clearly show the influence of traded parameters. The strikes are parameterized in terms of mass only, assuming a fixed relative velocity and for each spacecraft size a fixed lever arm from the center of mass (which is based on the overall size of the spacecraft). Also, the strikes are always applied about the x-axis. This allows the spacecraft response to to be characterized in one dimension as a function of the traded parameters only, allowing clear trends to emerge. For an analysis incorporating random strike direction and magnitude, see Bennett et. al.[16]

Spacecraft Size

Three design point spacecraft are developed to study the effects of spacecraft size on strike identification and assessment. The large spacecraft is NASA's Solar Dynamics Observatory, SDO, at approximately 2,000 kg. The medium spacecraft is Firesat, a notional spacecraft design of 215 kg. The third is a 12U cubesat at 24 kg. The detailed parameters used for each of the spacecraft are given in the appendix. The noise parameters are consistent across the three spacecraft and are loosely derived from noise observed in SDO's telemetry. Note especially that strikes are applied in terms of particle mass, and the distance between the strike and the center of mass (CoM) of the spacecraft is different for the different spacecraft sizes. Thus, a particle of a certain size striking SDO will impart substantially more angular momentum than the same particle striking the 12U cubesat since it is likely to hit significantly further from the center of gravity.

The results in Figure 7 show that smaller spacecraft can detect substantially smaller ΔHs. This is expected, since a smaller spacecraft has a lower moment of inertia so the same ΔH will impart more spin and be more easily detected. The detection rates in terms of particle size are also plotted, which take into account the shorter lever arm of the smaller spacecraft. The smaller two spacecraft still have lower detection thresholds than SDO, though the effects are less significant. The estimation accuracy is shown in Figure 7(c). Unsurprisingly, the spacecraft that can detect smaller strikes can also characterize the size of those strikes more accurately. Note that the discrepancies between simple and refined algorithms are minimal while the algorithms using momentum outperform the algorithms using attitude and rate by nearly an order of magnitude in all cases. This is especially noteworthy because calculating the inertial momentum incorporates the errors from both attitude and rate as well as wheel speed.

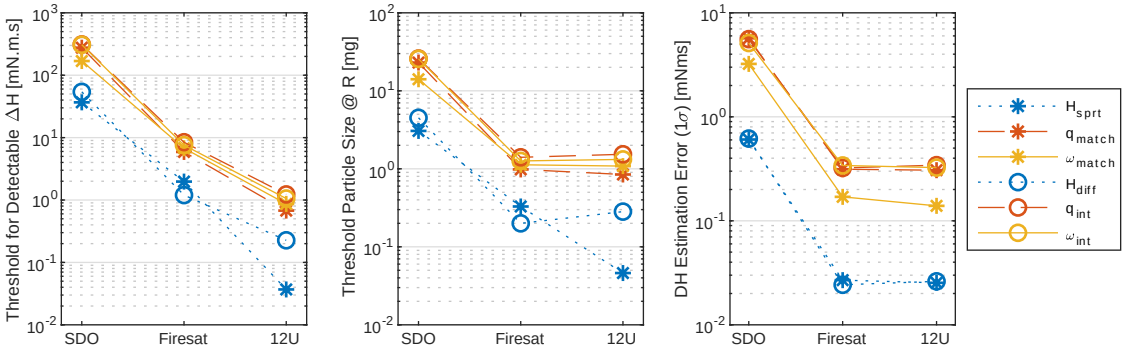

(a) Threshold in terms of ΔH (b) Threshold in terms of size (c) Estimation Accuracy

Figure 7. Trends in detection threshold for various S/C sizes

Telemetry Rate Trade

The simulation always runs at 100 Hz, but the telemetry is reduced to a lower rate representing downlinked telemetry. The default telemetry rate is 10 Hz. Since the dynamic spacecraft response to strikes lasts for about 25 seconds this provides a 250 point wavelet for the matched filters. The telemetry rate is traded but the length of the matched filters is left at 25 seconds, so the matched filters have more or fewer points at higher or lower telemetry rates. The momentum algorithms, however, work with a fixed length of 200 datapoints. The results are shown in Figure 8. As expected, the attitude and rate telemetry show notable degradation at lower telemetry rates since they have less data to work with. However, the momentum algorithms show little variation with telemetry rate. The attitude and rate filters approach the accuracy of the momentum filters at high data rates, but note that even with substantially more data (2500 points at 100 Hz vs 200 for the momentum algorithms) the momentum algorithms still perform better.

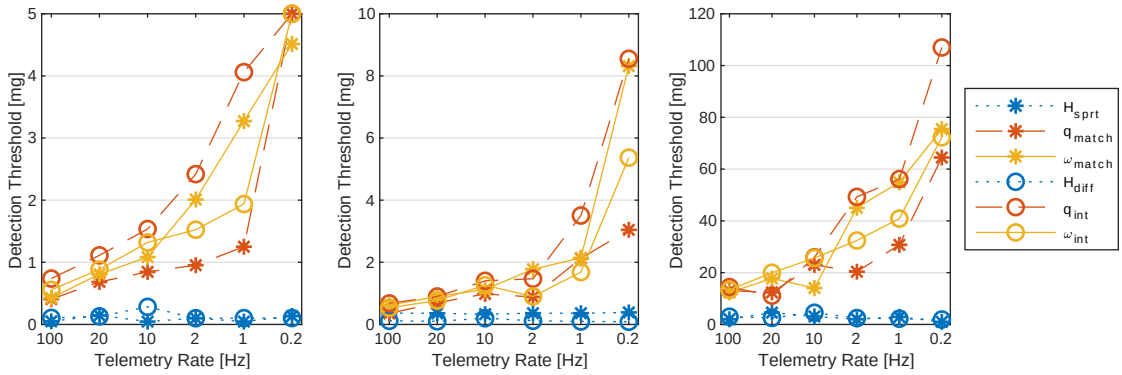

(a) 12U Cubesat (b) Firesat (c) SDO

Figure 8. Trends in detection threshold for various telemetry rates

Telemetry Noise Trade

All Telemetry Points The noise levels in all telemetry points are scaled to gain an understanding of the global effect of telemetry noise on algorithms. The noise is scaled up and down by a percentage of default noise applied on each telemetry point. The resulting thresholds show the expected trends with less noise resulting in lower thresholds and more noise resulting in higher thresholds (Figure 9). The results are somewhat muddy due to noise in the detection threshold measurement methods.

Trading Individual Telemetry's Noise While the momentum processing algorithms outperform the state error algorithms with the default noise levels, there are substantial differences in the accuracy of the rate measurement of various inertial measurement units. Therefore, trades are conducted where the noise levels in individual telemetry types are scaled to determine if the state algorithms can perform better than the

momentum algorithms given rate and attitude telemetry with lower noise, or wheel speed telemetry with higher noise. Figure 10 shows the results. The momentum processing algorithms still perform better with 10x the wheel speed noise (1σ = 24 RPM), after that performance degrades abruptly. The state algorithms begin to perform better with about order of magnitude reduction in noise (1σ = $\sim$0.825 arcsec/sec for rate, 1σ = $\sim$2.9 arcsec for attitude).

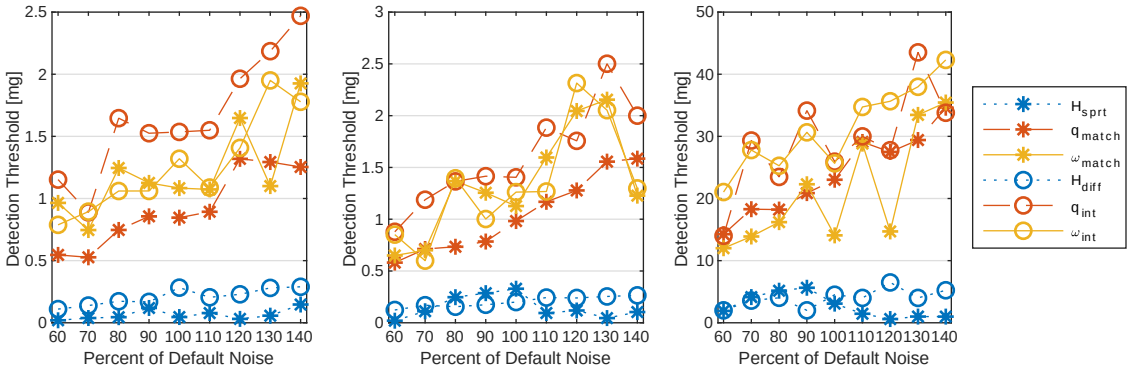

(a) 12U Cubesat (b) Firesat (c) SDO

Figure 9. Trends in detection threshold when trading telemetry noise

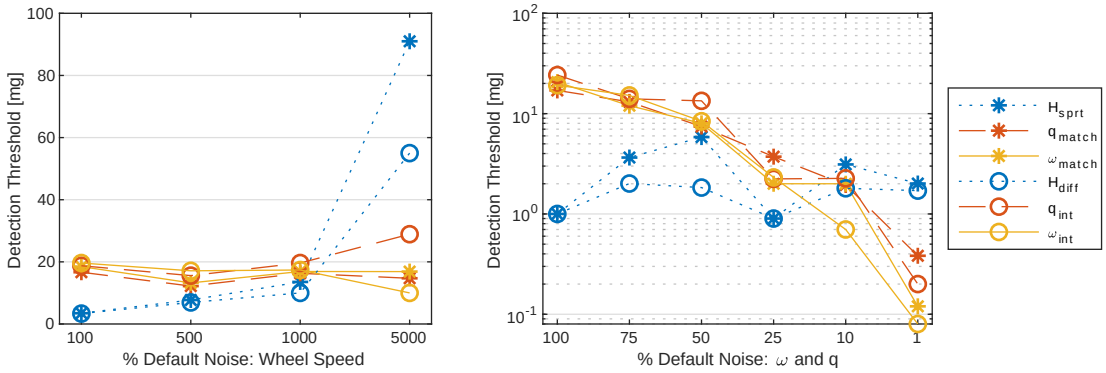

(a) Increasing Wheel Speed Noise (b) Lowering Rate and Attitude Noise

Figure 10. Trade noise in individual telemetry points (all data from SDO)

Other Trades

Three additional trades are conducted to see if they affect the results: the initial reaction wheel speed, the reaction wheel inertia, and the spacecraft inertia (Figure 11). The reaction wheel starting speed and inertia have no significant effect on the threshold, variations seem to be due to inherent noise in the process of setting the thresholds. The similarities between Figure 11(a) and Figure 11(b) are due to the random number generator in both runs having the same default seed, so the algorithms are working on the same random data. The spacecraft inertia changes the shape of the response wavelets which produces some minor changes in the thresholds, but these are relatively small for reasonable changes in inertia and are mostly overwhelmed with noise in Figure 11(c). All trades are made with SDO's default parameters.

DISCUSSION

Overall Trends

The results show that small spacecraft can detect substantially smaller strikes than large spacecraft, that a higher telemetry rate and lower noise can improve the strike detection threshold, and that the starting reaction wheel speed and reaction wheel inertia have minimal effect on the thresholds.

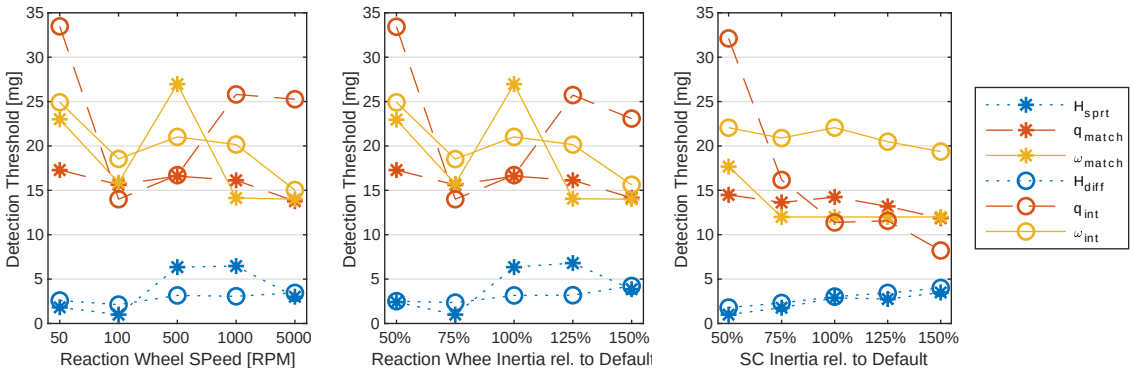

(a) Reaction Wheel Starting Speed (b) Reaction Wheel Inertia (c) Spacecraft Inertia

Figure 11. Trading miscellaneous spacecraft parameters

The results also showed that, while the momentum processing algorithms outperform the state error processing algorithms at the selected default noise levels, with substantially noisier measurements of reaction wheel speed the momentum algorithm performance is degraded. Similarly, reducing the noise in the attitude and rate measurements improves their performance significantly.

Surprisingly, the simple algorithms performed as well or sometimes better than the refined algorithms. The attitude matched filter was consistently the best among the state error processing algorithms, but not overwhelmingly so, and the SPRT performed comparably to differencing the averages in the momentum telemetry. This result should be caveated by mentioning that the non-Gaussian noise seen in real telemetry complicates setting an appropriate threshold, and the SPRT, with its ability to be tuned to ignore small effects, returns a substantially better signal-to-noise ratio on real data which is a non-trivial advantage. For this reason the SPRT is not discarded, even though performance is comparable on simulated telemetry while processing time is significantly slower.

Considerations for Real-World Application

As previously mentioned, these trades fixed several variables that would not be fixed in reality: the strike velocity, distance off the center of mass, and direction. This allowed the trades to be the only parameter varied to characterize the response of the algorithms to the traded parameters. However, in the real world the problem of determining the strike parameters from ΔH measurements is non-trivial - see the Future Work section below.

Another consideration is that the noise in these simulations is highly idealized. Perfect zero-mean white Gaussian noise is applied during the simulation to perturb the true state, and then perfect zero-mean white Gaussian measurement noise is added to the true state to produce the telemetry. In reality noise is much more complicated and can be colored, biased, non-Gaussian, and vary based on component temperature, wheel speed, and miscellaneous other effects which may or may not be fully characterized. Because of this, **these thresholds should be considered a best case scenario**; a real spacecraft's noise would be much harder to characterize accurately and consistently across all mission scenarios and therefore the detection thresholds would probably need to be raised to accommodate these variations.

In addition to difficulties in characterizing the baseline noise, experience has shown substantial unexpected events when processing on-orbit telemetry which obfuscate the debris strike detection results. For example, the momentum calculation assumes rigid body, so appendage vibration causes an apparent oscillation in the inertial angular momentum which trips the momentum detection threshold. Bennett and Schaub discuss examples of specific unexpected features seen in telemetry processed using these techniques[15].

Similarly, the momentum processing algorithms assume that the inertial angular momentum is unchanging relative to the minimum detectable threshold. In the simulated telemetry this is true, but in reality a spacecraft's momentum is constantly changing due to solar radiation pressure, etc. These changes must be

negligible relative to the detection threshold over the length of the window for the momentum processing algorithms to work effectively, which caps the length of window that can be used in practice.

While this paper refers to orbital debris as the impacting particle, in reality a large micrometeoroid would produce a nearly identical feature in telemetry, and in many orbits the flux of micrometeoroids exceeds that of orbit debris. Therefore, both populations must be taken into account when evaluating real-world impacts. Also, an electrostatic discharge has been proven to impart momentum to the discharging article[17], which, if large enough, could produce a comparable signature in ACS telemetry. To further complicate analysis, the momentum imparted by a hypervelocity impact is not equal to the relative momentum of the impacting particle - the effects of the impact include a high-velocity plume of ejected material spewing from the impacted surface, which can increase the imparted momentum by a factor of two or so.

While implementation challenges abound, these techniques show significant potential for giving improved methods to characterize the micrometeoroid and orbit debris environments using spacecraft as *in situ* debris sensors. Applying these techniques to SDO's momentum telemetry throughout 2016 and 2018 yielded patterns in strike count which repeated somewhat from year to year, indicating that they may be real events and not just telemetry noise. Comparing this data to the sporadic micrometeoroid flux[18] shows some interesting correlations in periods of higher and lower activity (Figure 12). Furthermore, for some of the larger events the results were checked individually to confirm that an abrupt momentum transfer occurred that was not caused by a predictable spacecraft event.

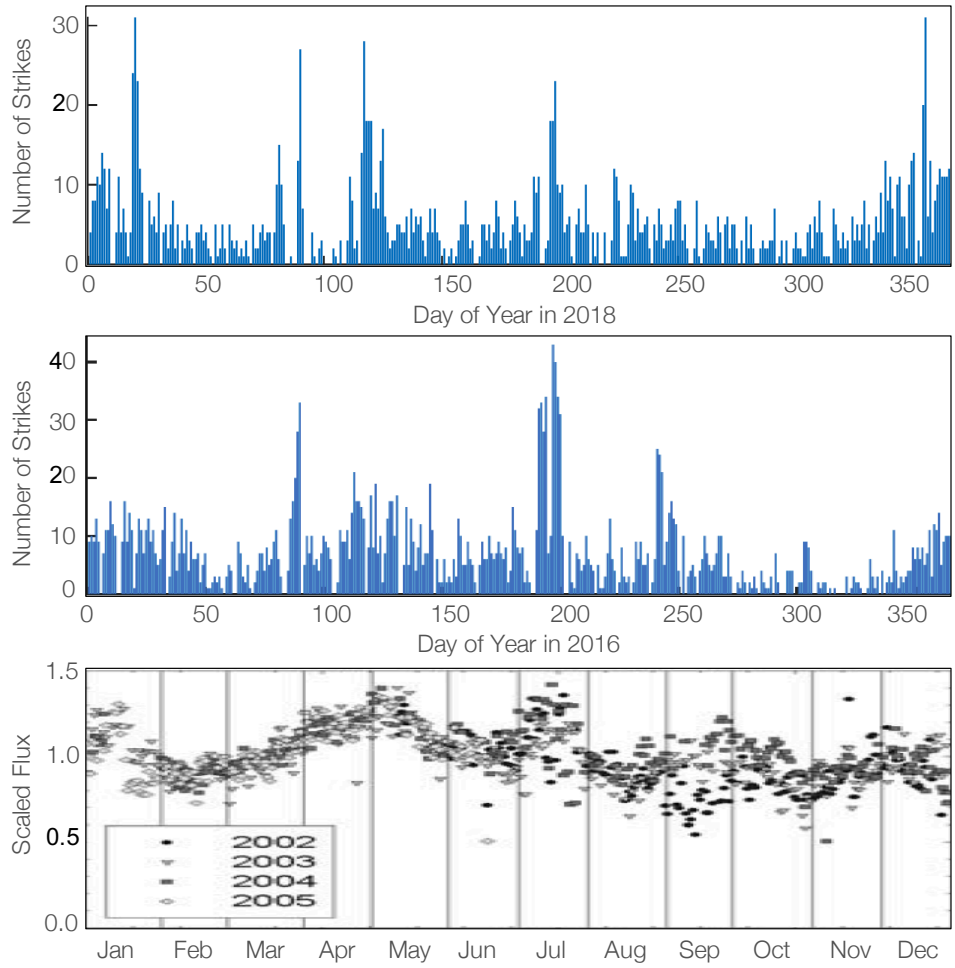

Figure 12. Initial results from SDO show some correlation to sporadic micrometeoroid flux

Future Work

Additional years of SDO data will be processed to see if the same trends continue to appear, and those results will be compared to the expected flux based on micrometeoroid models. In addition to SDO, data from several other NASA space science missions will be processed to see if similar trends can be found. These include Earth-orbiting spacecraft in LEO and HEO as well as interplanetary spacecraft and the Lunar Reconnaissance Orbiter. This diversity in orbits offers a unique opportunity to observe whether the potential micrometeoroid flux correlation is repeatable for non-Earth orbiting spacecraft, and whether Earth-orbiting spacecraft experience events consistent with their modeled debris environments.

As mentioned above, translating from a ΔH measurement to specific debris parameters is non-trivial, since ΔH is the cross product of the strike location relative to the center of mass crossed with the mass times the relative velocity. This results in one equation with three unknowns. However, a three-axis measurement of the ΔH vector can define a plane of the impact, which helps to define possible strike location, and orbit debris is most likely to hit from the ram direction while micrometeoroids also show preferred directions, although they vary annually. So one ΔH measurement cannot be used to solve for strike parameters, but combining a population of ΔH measurements with known fluxes and spacecraft geometry it might be possible to fit a mass distribution to the debris flux that maximizes the likelihood of obtaining the observed data. Methods to develop this estimation will be pursued.

CONCLUSIONS

The trades performed in this study illustrate the effect that various spacecraft and noise parameters have on the effectiveness of these algorithms. While this study makes some idealized assumptions the general trends inform the strike detection capabilities of various spacecraft with various ACS suites. The results from SDO, especially when compared with the annual sporadic fluxes, provide some evidence that these techniques can be used to gain a better understanding of the micrometeoroid and orbital debris environment that a spacecraft is flying in.

ACKNOWLEDGMENT

This work was supported by a NASA Space Technology Research Fellowship, NASA grant 80NSSC18K1142.

REFERENCES

[1] "Monthly Number of Objects in Earth Orbit by Object Type". In: *Orbital Debris Quarterly News* Volume 23.1 (May 2019).

[2] James Shell. "Optimizing orbital debris monitoring with optical telescopes". In: Advanced Maui Optical and Space Surveillance Technologies Conference. Maui, HI, Sept. 14, 2010.

[3] E. Christiansen et al. "Reaction of Spacecraft Batteries to Hypervelocity Impact". In: *Orbital Debris Quarterly News* 21.1 (Feb. 2017).

[4] *Space Debris by the Numbers*. European Space Agency. `https://www.esa.int/Our_Activities/Space_Safety/Space_Debris/Space_debris_by_the_numbers`, (accessed 8-6-19).

[5] P. Krisko. "The New NASA Orbital Debris Engineering Model ORDEM 3.0". In: 2014 Astrodynamics Specialist Conference. San Diego, CA: NASA Technical Report JSC-CN-30742, Aug. 4–7, 2014.

[6] Stephen Clark. "Investigators conclude external forces killed an Intelsat satellite in April". In: *Spaceflight Now* (July 30, 2019).

[7] H. Krag et al. "A 1 cm space debris impact onto the Sentinel-1A solar array". In: *Acta Astronautica* 137 (Aug. 2017), pp. 434–443.

[8] Trevor Williams, Joseph Sedlak, and Seth Shulman. "Magnetospheric Multiscale Mission Micrometeoroid/Orbital Debris Impacts". In: Spacecraft Anomalies and Failures Workshop 2017. Chantilly, VA, Dec. 12, 2017.

[9] G.A. Graham et al. “The chemistry of micrometeoroid and space debris remnants captured on hubble space telescope solar cells”. In: *International Journal of Impact Engineering* 26.1 (Dec. 2001), pp. 263–274.

[10] Michael Squire. “Micrometeoroid and Orbital Debris Testing on Composite Overwrapped Pressure Vessels”. 2019 Applied Space Environments Conference. Los Angeles, CA, May 15, 2019.

[11] *Evaluation of Micrometeoroid and Orbital Debris (MMOD) Risk Predictions with Available On-orbit Assets*. NASA Engineering and Safety Center Technical Assessment Report NESC-RP- 14-01000. NASA Engineering and Safety Center, Oct. 13, 2017.

[12] Brien Flewelling et al. “Explained and Unexplained Momentum Impulse Transfer Events”. In: 7th European Conference on Space Debris. Darmstadt, Germany: ESA Space Debris Office, Apr. 18, 2017.

[13] Joel Williamsen et al. “Characterizing the Orbital Debris Environment Using Satellite Perturbation Anomaly Data”. In: First International Orbit Debris Conference. Sugarland, TX, Dec. 9–12, 2019.

[14] Robin Putzar et al. “How Hypervelocity Impacts Can Affect the LISA Mission – The MIRAD Study”. In: International Astronautical Congress. Washington, D. C., October 21 - 25, 2019.

[15] Anne Aryadne Bennett and Hanspeter Schaub. “Identifying and Assessing Debris Strikes in NASA Spacecraft Telemetry”. In: First International Orbit Debris Conference. Sugarland, TX, Dec. 9–12, 2019.

[16] Anne Aryadne Bennett, Hanspeter Schaub, and Russell Carpenter. “Assessing Debris Strikes in Spacecraft Telemetry: Development and Comparison of Various Techniques”. In: 70th International Astronautical Congress. Washington, D. C., Oct. 21–25, 2019.

[17] Alexander L. Bogorad et al. “Electrostatic Discharge Induced Momentum Impulse From Charged Spacecraft Surfaces”. In: *IEEE Transactions on Nuclear Science* 53.6 (Dec. 2006), pp. 3607–3609.

[18] M. D. Campbell-Brown and J. Jones. “Annual variation of sporadic radar meteor rates”. In: *Monthly Notices of the Royal Astronomical Society* 367.2 (Apr. 2006), pp. 709–716.

APPENDIX: DEFAULT VALUES FOR PARAMETERS

Spacecraft Parameters

Parameter	SDO	Firesat	12U
S/C Mass [kg]	2000	215	24
S/C Inertia$_{xx}$ [kg.m^2]	3000	65	1.85
S/C Inertia$_{yy}$ [kg.m^2]	2500	55	1.5
S/C Inertia$_{zz}$ [kg.m^2]	3500	90	2.5
RW Inertia [kg.m^2]	0.16	.0011	5.15E-5
RW Max Torque [N.m]	0.2	0.03	0.002
$R_{\text{debris-COM}}$ [m]	1.5	0.75	0.1

Noise Parameters

Parameter	Value	Unit
Noise in applied torque	σ=0.005*T_{max}	N.m
Noise in attitude tlm.	σ=7E-5	-
Noise in rate tlm.	σ=4E-5	rad/s
Noise in RW speed tlm.	σ=0.25	rad/s
RW speed resolution	0.1	rad/s
Default tlm. rate	10	Hz